

Plastic load bearing capacity of multispan composite highway bridges with longitudinally stiffened webs

Harald Unterweger*, Andreas Lechner and Richard Greiner

Institute of Steel Structures, Graz University of Technology, Lessingstraße 25, A - 8010 Graz, Austria

(Received April 28, 2010, Accepted November 09, 2010)

Abstract. The introduction of the Eurocodes makes plastic design criteria available also for composite bridges, leading to more economical solutions compared with previous elastic design rules. Particularly for refurbishment old bridges with higher actual traffic loads, up to date outside the scope of the Eurocodes, strengthening should therefore be avoidable or at least be necessary only to a minor extent. For bridges with smaller spans and compact cross sections, the plastic load bearing capacity is clearly justified. In this work, however, the focus is placed on long span continuous composite bridges with deep, longitudinally stiffened girders, susceptible to local buckling. In a first step, the elastic - plastic cross section capacity of the main girder in bending is studied as an isolated case, based on high preloads acting on the steel girder only, due to the common assembling procedure without scaffolding. In a second step, the effects on the whole structure are studied, because utilising the plastic section capacity at midspan leads to a redistribution of internal forces to the supports. Based on the comprehensive study of an old, actual strengthened composite bridge, some limitations for plastic design are identified. Moreover, fully plastic design will sometimes need additional global analysis. Practical recommendations are given for design purposes.

Keywords: plastic moment capacity; nonlinear global analysis; existing composite highway bridges.

1. Introduction

The comprehensive studies presented in this paper are based on the conditions of the majority of long span continuous composite girder bridges in Central Europe:

- continuous plate girders with longitudinal and vertical stiffeners and constant girder depth,
- continuous concrete deck above the steel section with uninterrupted shear connectors over the whole bridge length,
- un - propped structures, that means erection without scaffolding, leading to high normal stresses in the steel girder before composite action, due to dead loads of steel and concrete deck,
- in general the design is based on elastic global analysis and elastic cross section resistance, without consideration of slip in the interface between structural steel and concrete deck.

Effects due to creep and shrinkage and concreting sequence are neglected in this study. Based on these facts, the design is based on the typical elastic stress distributions shown in Fig. 1. For better understanding, only one main girder - representing the global behaviour of the bridge deck - is considered. Because of the different behaviour, sections in span and near the internal supports must be di-

* Corresponding author, Professor, E-mail: h.unterweger@tugraz.at

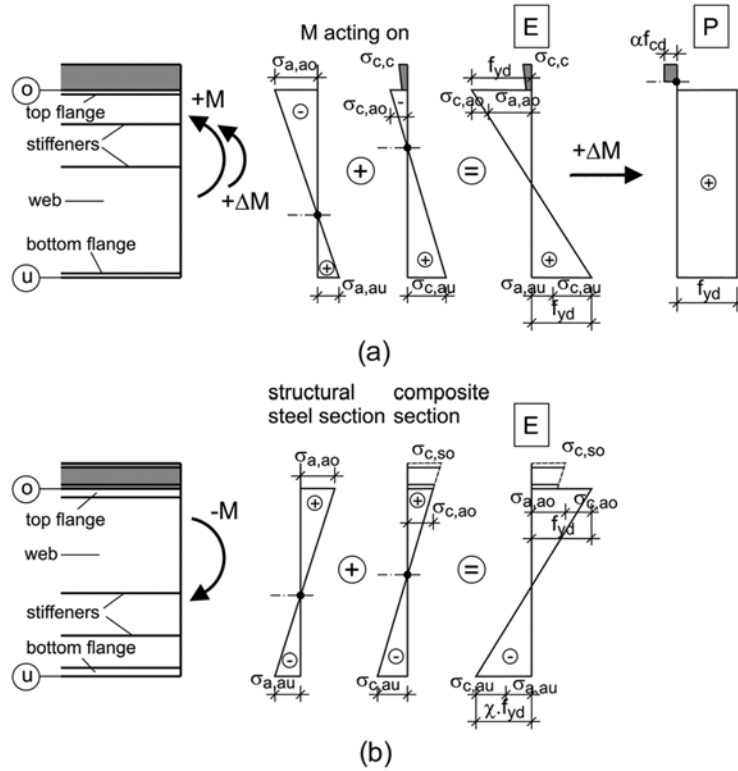


Fig. 1 Cross section in bending; (a) in span near midspan (section m), (b) at internal support (section s)

stinguished. In this paper, the two representative sections, m at midspan and s at the internal support are considered in most cases. In both sections, high stresses due to moments M_a , acting on the structural steel section only, can be observed (stresses $\sigma_{a,i}$ due to dead loads of structural steel and concrete deck). For the moments M_c , acting on the composite section, the concrete deck contributes only in span (sagging moments), whereas at the internal support - in a simplified treatment - only the reinforcing steel is active (hogging moments).

In the following the symbols in general are based on the Eurocode definitions, but for stresses due to moments M_a , acting on the structural steel only, an additional first index a and for moments M_c , acting on the composite section, an additional first index c is used. The second index indicates the member (a = structural steel, c = concrete, s = reinforcing steel) and the suffix o and u represents top and bottom fibre respectively (e.g., $\sigma_{a,ao}$, $\sigma_{c,au}$).

Superposition of the two components - M_a and M_c at midspan - leads to the elastic moment capacity $M_{0,Rd}$, when the maximum stress reaches the limiting yield stress f_{yd} (sometimes reduced to the value of $\chi \cdot f_{yd}$ based on buckling of the compression flange and web respectively). At the internal support, an additional plastic section capacity is very limited and is therefore ignored in the following. This fact is based on the effects of the high shear forces, the buckling limits of the stiffened web (column - like behaviour) and the negligible tension resistance of the concrete deck. These limits, in contrast, are not relevant for the sections m in span and, therefore, utilising the plastic section capacity should lead to significant additional moments ΔM acting on the composite section (Fig. 1(a)).

Use of Eurocode 4 (2007) allows to apply the plastic moment capacity for composite bridges in ge-

neral, considering a reduction of the design value of the cylinder compressive strength of concrete f_{cd} by a factor $\alpha = 0,85$. For bridges with short spans and low girder depths buckling of the webs is usually not relevant and the plastic moment capacity in span is useable. Moreover, a moment redistribution could be also taken into account for the sections at the internal supports, leading to plastic design procedures. For building constructions they are well established (e.g., Johnson and Chen (1991), recently Chen and Jia (2008)) and also for more general application of continuous composite beams (e.g., Couchman and Lebet (1996)). But also for bridge application detailed studies were made (e.g., Johnson and Huang (1995), particularly by Lääne and Lebet (2005a)). Worth mentioning in the last paper is the utilisation of the plastic rotation capacity at the internal supports, specified in detail in Lääne and Lebet (2005b), leading to favourable moment redistributions.

In this paper this field of application, well understood and prepared for practical work (e.g., Ducret and Lebet (2001)), should be widened including girders with high depths and slender webs with longitudinal stiffeners. Utilising the additional plastic moment capacity in span should mainly be beneficial for refurbishment of old bridges, to avoid strengthening or at least be necessary only to a minor extent. A detailed study - also for the bending behaviour of the cross section in span - was necessary, because the column like behaviour of stiffened webs (e.g., Maquoi and Skaloud (2000)) to the authors knowledge was not studied so far (e.g., Fournier, *et al.*, (1994) studied very slender webs without longitudinally stiffeners). Therefore a comprehensive study was carried out based on the geometry and the sections of an old continuous highway bridge in Austria, erected in 1974. The basic results were elaborated in a diploma thesis by G. Utenthaler (2008). It is worth to mention that an assessment of old bridges is outside the scope of Eurocodes, but they may be used for this purpose if material and workmanship meet the requirement of the relevant Euronorms.

In Fig. 2 the overview of the studied composite highway bridge is summarized. There are two individual concrete decks for each carriageway, but the four main girders act together as a grillage due to cross bracings ranging over the full width. The eleven spans of the real bridge are reduced in the analysis, leading to a continuous symmetric girder bridge with three spans and span lengths of $L_1 = 56$ and $L_2 = 80$ m respectively. The plate thicknesses (web, top and bottom flange) for the analysed outer main girder in axis D are summed up in Fig. 2(b) and the sections at midspan and at the inner support are shown in Fig. 2(c). The three longitudinal stiffeners are omitted here. In the figure also the modified symmetric concrete deck is shown, which leads to the same normal stresses for vertical loads as when considering the effective width of the concrete deck. This was necessary, due to the asymmetry of the actual concrete deck. At the internal support the reinforcing steel (about 1,4% of concrete area) has been increased in the computer model due to the *tension stiffening effect*.

The main aspects of utilising the plastic moment capacity for this typical composite bridge with slender sections, susceptible for local web buckling, are as follows:

- utilisation of the plastic moment capacity in the field section m ,
- redistribution of bending moments due to plastification in midspan, leading to increased moments in other sections.

2. Plastic moment capacity in span (sagging moments)

2.1 Boundary conditions and simulation model

In Fig. 3 the boundary conditions for the analysed main girder in axis D are summed up. The

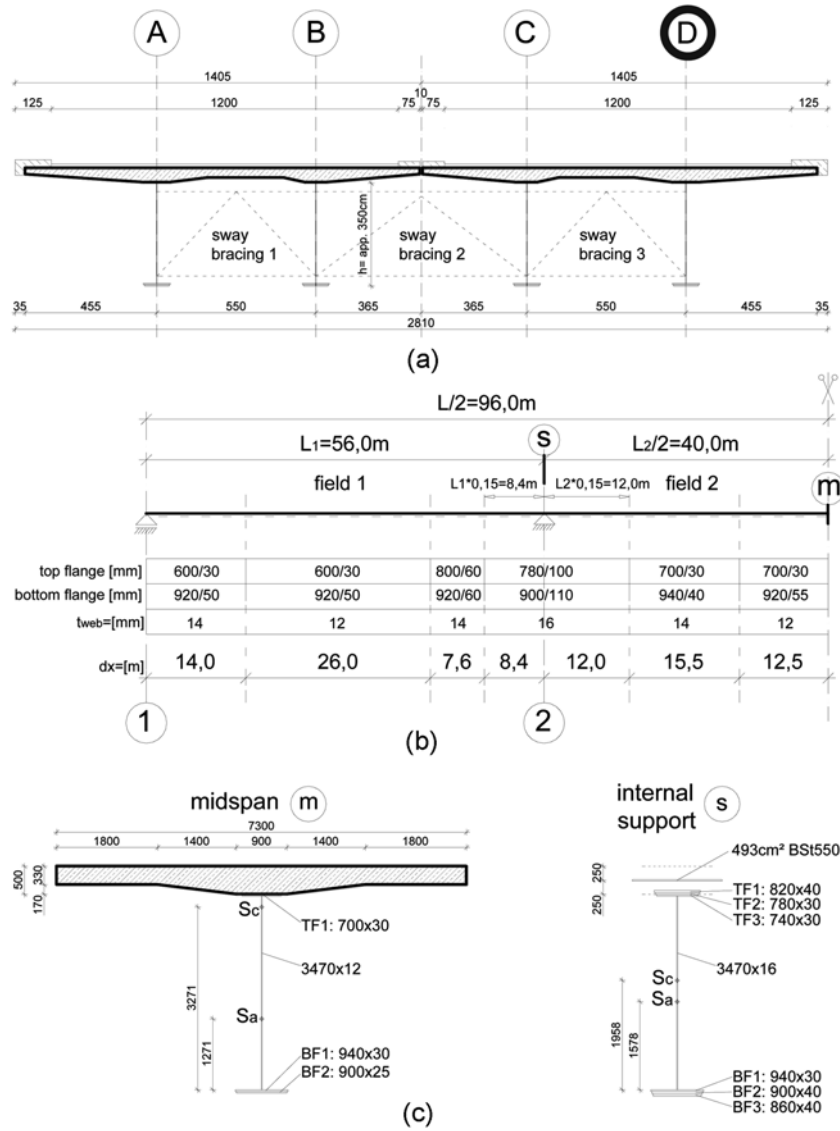


Fig. 2 Details of the studied composite highway bridge; (a) cross section of the bridge, (b) dimensions for main girder D, (c) cross section at midspan and at internal support

characteristic yield strength of the fine grain steel is $f_{yk} = 410 \text{ N/mm}^2$. Based on the load and resistance factor design in Eurocode, with $\gamma_M = 1,1$ (the bending capacity is influenced by stability effects), a design value of $f_{ydl} = 373 \text{ N/mm}^2$ is obtained. The concrete of class C 30 / 37 in Eurocode has a characteristic compressive strength of $f_{ck} = 30 \text{ N/mm}^2$ and leads to a ratio of the moduli of elasticity $E_a / E_c = 6,56$. The reinforcing steel in span is neglected.

The web of the plated girder, with a depth of about 3,5 m and a thickness of 12 mm, is stiffened by three hollow longitudinal stiffeners (cold formed L-stiffeners with a thickness of 6 mm). The distance between the vertical stiffeners is $a = 3 \text{ m}$. Their bending stiffness is very high and, they act therefore

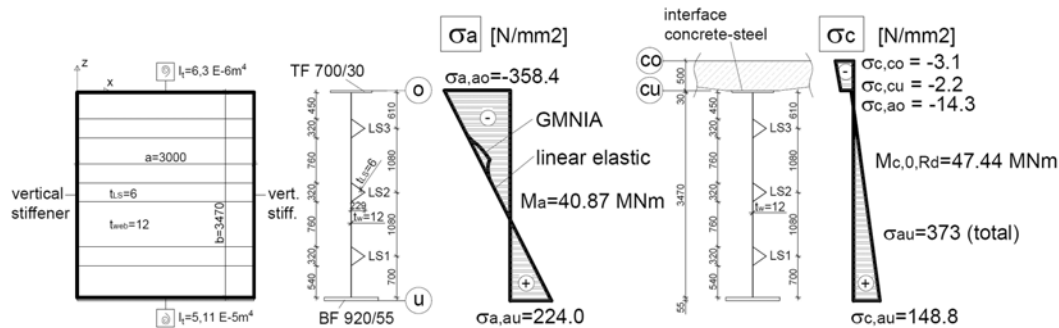


Fig. 3 Details for calculation of the bending cross section capacity at midspan

like rigid out-of-plane supports for the web. For loads acting on the structural steel section only, before composite behaviour is developed, the major part of the web is under compression (stress distribution σ_a in Fig. 3). The high slenderness of the web and the longitudinal stiffeners leads to web buckling and, therefore, the elastic bending resistance of the structural steel section is not fully attainable (classified as class 4 in Eurocode).

The dead loads of the structural steel and the concrete deck (amplified by a partial safety factor of $\gamma_F = 1,35$) for the studied structure - acting on the structural steel section only - lead to normal stresses on the top flange of about 65% of the design yield strength (the details of the global analysis are given in chapter 3). To get an upper bound of steel - stresses before composite action, these dead loads were increased to a maximum of about 96% f_{ydb} leading to the elastic stress distribution σ_a in Fig. 3. Those may be considered as limiting values for practical application. In the following loads and bending moments, which only act on the structural steel section are called “preloads”.

The numerical FE - model, based on the software ABAQUS (2007), consists of a segment of the main girder between two vertical stiffeners in order to study the influence of local buckling on the resistance of the structural steel section. The web and the longitudinal stiffeners are modelled with shell elements (type “S8EL”, with parabolic deformation functions). The detailing can be seen in Fig. 4(a). The flanges are modelled with beam elements. Their torsional stiffness (Fig. 3) was also used as an input parameter for the software EB - Plate (2006), to check the buckling eigen - values. The concrete deck was modelled with two beam elements (for the region of variable thickness and the region with constant thickness respectively), leading to nearly the same results as using plate elements.

The boundary conditions and the loading of the model turned out to be worth mentioning. Along the vertical stiffeners all elements are linked, so that the sections remains plane also after deformation and no slip at the interface between concrete and structural steel occurs. The bending moment was introduced by two forces, acting at the flanges. These forces are always acting perpendicularly to the end section, leading to lateral compression in the web between the ends, due to the high curvature of the girder segment. For the material behaviour different approaches were studied (with / without steel hardening and with concrete in tension respectively), which led to nearly the same section capacities.

In the first load step the bending moment acting on the structural steel section was applied. To capture local buckling effects, a geometrically and materially nonlinear analysis with imperfections was carried out. The equivalent geometric imperfections were based on the calculated eigenmodes, as recommended in Eurocode 3 (2007). A background of this code, specifying plate buckling behaviour, is given in Johannson, *et al.* (2001). In Fig. 4a the first local eigenmode (buckling occurs between the two upper

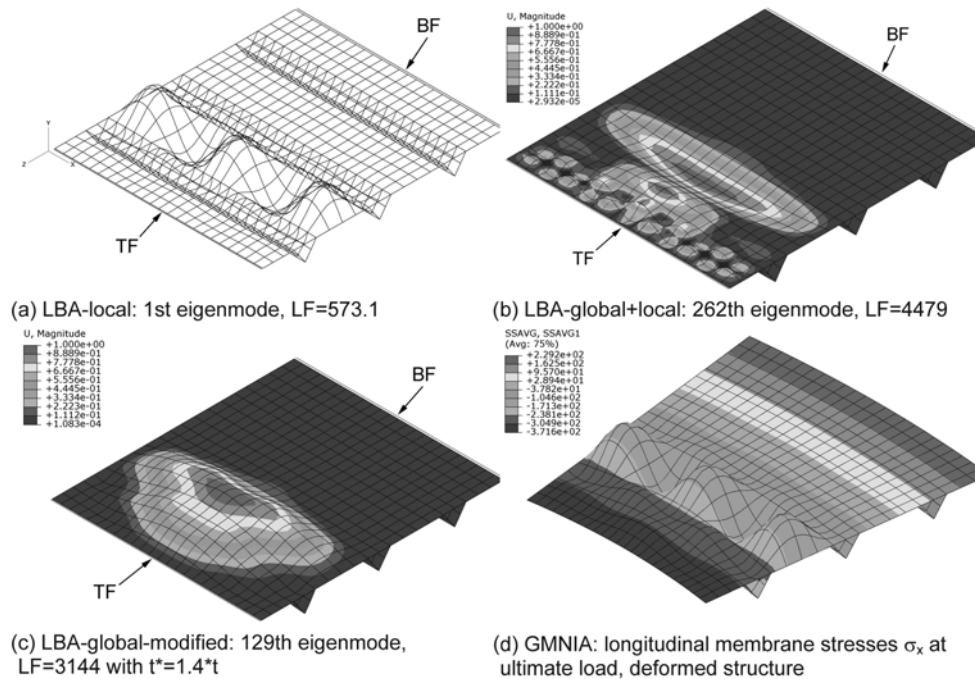


Fig. 4 GMNIA - analysis of midspan steel girder section; (a) local, (b) global, (c) modified global buckling mode. (d) field of longitudinal normal stresses at ultimate load

longitudinal stiffeners) is presented. The first global eigenmode, in form of superposed local and global submodes (local - global in Fig. 4 (b)) cannot be used directly. Therefore, an additional calculation with a thicker web was made, to eliminate the superimposed local eigenmodes, leading to the modified form in Fig. 4(c). The local and modified global eigenmode were scaled, based on the maximum equivalent imperfection values in annex C of Eurocode 3 (2007) (local: $b_{EF} / 200 = 760 / 200 = 3,8 \text{ mm}$; global: $a / 400 = 3000 / 400 = 7,5 \text{ mm}$), and they were superposed without any reduction (one of both would allowed to be reduced by 30 % according to Eurocode 3). The load factors (LF) in Fig. 4 may be considered as equivalent to the calculated ideal buckling stresses σ_{cr} in N/mm^2 .

The deformations and normal stresses of the web, resulting from the GMNIA - analysis (geometric and material nonlinear analyses with imperfections) for the loads acting on the structural steel section, are shown in Fig. 4(d). Due to local buckling, a decrease of the normal stresses between the two upper longitudinal stiffeners, in contrast to the linear elastic distribution, can be identified, as shown in Fig. 3. Nevertheless, nearly the full elastic resistance of the structural steel section is reached.

In the second load step the concrete slab was activated on the pre - loaded girder and the bending moment was increased. In Fig. 5 the stress - strain relationship used for concrete and structural steel is shown. Two independent calculations were made, based on the characteristic and on the design resistances respectively. The partial safety factors for the latter ones, in accordance with the Eurocode, are given in Table 1 and 2. The increase of the steel stresses beyond the yield stress in Fig. 5(b) is not considered due to the strain hardening effect but due to the true stress - strain relationship in the FE - model.

In Table 1 and 2 the calculated moment capacities (sagging moments) are summed up. Table 1 gives

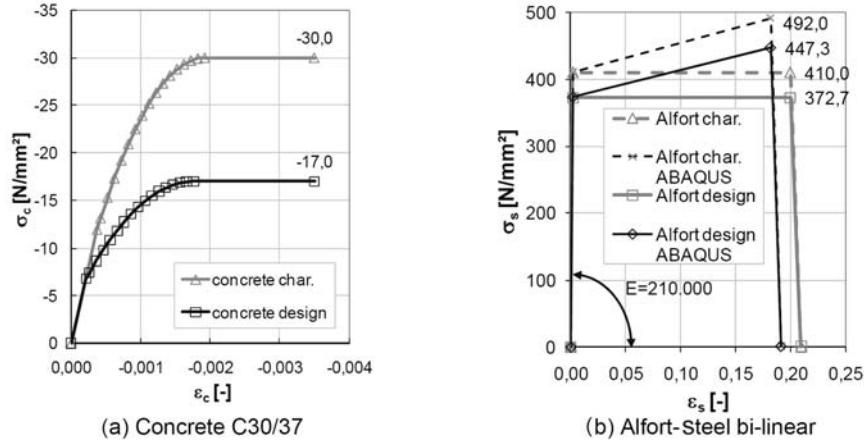


Fig. 5 Stress - strain relationship for (a) concrete, (b) structural steel, in the nonlinear calculations

Table 1 Bending cross section capacity at midspan - analytic results

Basis	M_a [MNm]	$M_{c,0}$ [MNm]	M_{total}				
			$M_{0,Rd}$ [MNm]	$M_{el,Rd}$ [MNm]	$M_{pl,Rd}$ [MNm]	$M_{0,Rd}/M_{pl,Rd}$ [-]	$M_{el,Rd}/M_{pl,Rd}$ [-]
char. value $\gamma_{Mi} = 1,0$	44,96 (96% f_{yk})	52,18	97,14	105,54	130,12	0,747	0,811
design value $\gamma_{M0} = \gamma_{M1} = 1,1$ $\gamma_C/\alpha = 1,765$	40,87 (96% f_{yd})	47,44	88,31	95,95	114,95	0,768	0,835

Table 2 Bending cross section capacity at midspan - GMNIA results

Basis	M_a [MNm]	M_c [MNm]	M_{total}	
			$M_{GMNIA,pl,Rd}$ [MNm]	$M_{GMNIA,pl,Rd}/M_{pl,Rd}$ [-]
char. values $\gamma_{Mi} = 1,0$	46,61(100% f_{yk})	83,54	130,15	1,00
design values $\gamma_{M0} = \gamma_{M1} = 1,1$ $\gamma_C/\alpha = 1,765$	42,40(100% f_{yd})	71,72	114,12	0,993

the analytical results and Table 2 shows the results of the GMNIA - calculation with the FE - model. There is a little difference in the pre - load level (acting on the structural steel section only), however, this is not relevant for the final results.

The GMNIA analysis (also if strain hardening of the structural steel is neglected) gives a moment capacity which is nearly the same as the analytical full plastic moment capacity for the composite section. In the Tables the moment M_a acting on the structural steel section, the additional moment M_c on the composite section and the superposed moment capacity M_{total} is presented. The moment $M_{0,Rd}$ is the elastic resistance of the section, based on the superposed normal stresses due to loads on the structural steel section and composite section, shown in Fig. 1. $M_{el,Rd}$ and $M_{pl,Rd}$ are the elastic and plastic moment capacities of the composite section respectively, ignoring the preload on the structural steel section. In spite of little differences in preload level and individual calculations with characteristic and design values the resulting moment capacities (M_{GMNIA} / M_{pl}) are nearly the same.

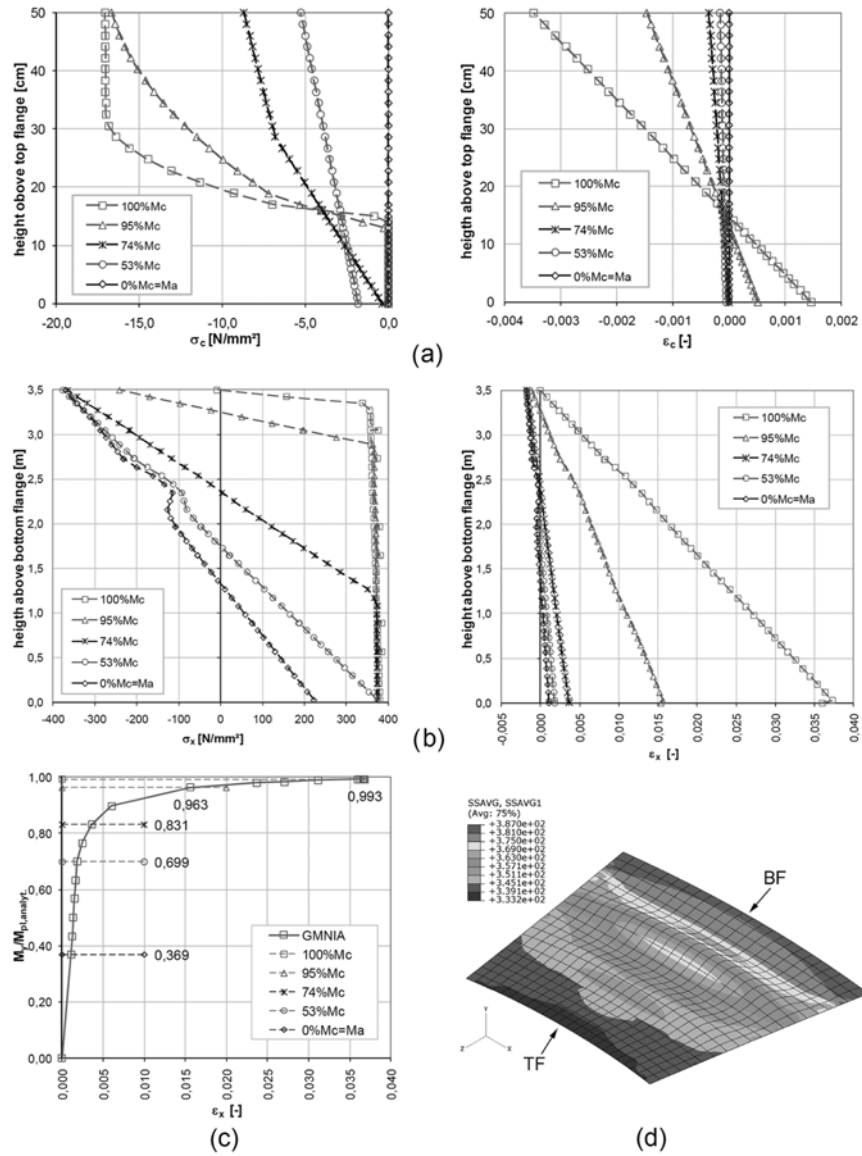


Fig. 6 GMNIA - results for cross section at midspan; (a) and (b) normal stresses and associated strains in concrete slab and girder web respectively; (c) Tension strains at bottom flange related to bending moment M_c on composite section; (d) normal stresses of girder web at ultimate load

Increasing the load to nearly the full plastic moment capacity of the composite section leads to high tension stresses in the structural steel section - also near the top flange - and the position of the neutral axis rises into the concrete slab. This can be seen in the stress- and strain distributions of the concrete slab and the structural steel section in Fig. 6. In addition, distributions for different load levels of M_c , starting with the preload condition ($M_c = 0$) are illustrated. The region of the steel web, susceptible to local buckling due to preloads, cannot attain further compressive strains and, therefore, a plastic stress redistribution is possible.

The deformed web with the normal stresses at ultimate load level is shown in Fig. 6(d). The variation of the normal stresses along the girder length is based on superposed compressive stresses perpendicular to the girder axis due to the high curvature. The dramatic increase of the section curvature for moments reaching the full bending capacity (Fig. 6(c)) discussed in detail in the following, is also obvious when looking at the longitudinal strains in the bottom flange in Fig. 6(b).

In summary, the utilisation of nearly the full plastic moment capacity of the composite section is possible, also for composite sections with slender webs that are highly stressed and susceptible to local buckling due to preloads acting on the structural steel section. To verify this behaviour also for slender longitudinal stiffeners, which lead to more significant global buckling effects including buckling of the stiffeners, an additional study was made, based on the main dimensions of the girder-web-panel in Fig. 3. In Table 3 the results of two of the analysed modified cases are summed up. One case deals with longitudinal stiffeners of reduced depth ($h_s = 126$ mm) and one case with an additional longer distance between the vertical stiffeners ($a = 4500$ mm). To characterise the buckling behaviour of the longitudinal stiffener, acting as a pin-ended column between the vertical stiffeners, its non-dimensional slenderness $\bar{\lambda}_{c,s}$ is also listed. Its calculation is based on the full cross section area of the stiffener including the web plate ($\bar{\lambda}_{c,s} = \sqrt{f_y / \sigma_{cr,s}}$). The results - based on an analysis with design values - are compared with the actual panel behaviour (results of the last row in Table 2). In addition to the moment capacity $M_{a,Rd}$ the deformation $u_{a,max}$ transverse to the web-plane of the topmost longitudinal stiffener (in the middle of the panel) due to the preload effects ($M_a \sim 0,9 M_{a,Rd}$) is presented. The moment capacity $M_{GMNIA,pl,Rd}$ is the calculated ultimate load associated with the deformation u_{max} of the longitudinal stiffener, considering the preload effect. It could be found, that - in spite of additional moments M_c acting on the composite section - beneficial tension stresses in the web-plate are activated, which lead to a reduction of the out-of-plane deformations u_{max} of the longitudinal stiffener.

Therefore, also for the modified web panels with very slender longitudinal stiffeners - susceptible to buckling out-of-plane - and high preloads, nearly the full plastic moment capacity $M_{pl,Rd}$ of the composite section is available. It must be said that the calculated moment capacities are conservative, because the boundary condition allows free bending of the longitudinal stiffener out of the web-plane and leads to a load application to the web plate only, resulting in additional out-of-plane deformations.

It is, however, obvious that very high plastic strains are necessary to activate the plastic moment capacity leading to high cross-sectional curvature. Therefore, it must be checked, whether the associated redistribution of the bending moments of the continuous girder towards the internal supports leads to a significant increase of the design moments based on an elastic analysis. Through the dramatic increase of curvature near the ultimate capacity, plastic utilisation in design (e.g., limitation to 90%) will be restricted and will reduce the amount of moment redistribution in practice.

These questions are discussed in detail in the next chapter, based on a nonlinear global analysis for the studied bridge structure, including the checking of the moment redistribution for the other sections.

Table 3 Bending cross section capacity at midspan for modified web panels - GMNIA results

case	a [mm]	h_s [mm]	$\bar{\lambda}_{c,s}$	$M_{a,Rd}$ [MNm]	$u_{a,max}$ [mm]	$M_{GMNIA,pl,Rd}$ [MNm]	$M_{pl,Rd}$ [MNm]	$M_{GMNIA,pl,Rd} / M_{pl,Rd}$ [-]	u_{max} [mm]
actual panel	3000	229	0,85	42,40(100%)	0,5	114,12	114,95	0,993	6,9
mod 1	3000	126	1,21	37,47(89,8%)	22,7	111,67	113,13	0,987	3,0
mod 2	4500	126	1,48	33,48(80,2%)	30,1	111,94	113,13	0,989	2,6

3. Moment redistribution due to utilisation of the plastic section capacity at and near midspan

3.1 Model for global analysis

In addition to an elastic global analysis also a nonlinear analysis for the main girder D was performed to study the moment redistribution with increasing utilisation of the plastic section capacity in span. In the model only the main girder D is treated. Therefore, the elastic influence lines for the whole structure were developed in a pre-study to find the correct traffic load-condition in the model (distributed load p , single load P) due to traffic loads on different lanes. The stiffness distributions of the main girder D were based on the material distribution in Fig. 2. Different distributions had to be accounted for the preload - applied fully on the structural steel sections only - and the loads acting on the composite sections. For the latter ones the length of the cracked zone of the concrete deck was simplified using 15% of the adjacent span length (this gives a total length of 20,4 m, see Fig. 2). The *tension stiffening effect* was taken into account by an increased area of the reinforcement (about + 30%), leading to a fictitious total reinforcing ratio of 1,8% of the concrete area (this effect can be neglected in Eurocode 4 (2007) for the stiffness calculation in the global analyses). The global analysis was made for the traffic load model 1, according to Eurocode 1 (2003) and for the Austrian national traffic load model (ÖNORM (1970), RVS (1999)). For this example the first one leads to about 20% higher design moments. The reason for considering the national load model was, that the real design of the bridge structure had to be based on this model. In cases where the results of the nonlinear calculations for the national load model could not be generalized also for the European load model, additional calculations for the latter one (Eurocode 1 (2003)) were made.

The elastic global analysis was carried out with a beam model, whereas the nonlinear calculations were made by a combined model with shell and beam elements, similar to the study for the non-linear bending capacity of the section. However in contrast, the buckling effects of the web were ignored and, therefore, the longitudinal stiffeners and the geometric imperfections of the web were neglected. Ignoring the local buckling effect was justified by checking the moment - curvature relationship for the sections, which led to similar values as before. However, comparing the moment capacities of the sections in detail a little bit different values than in chapter 2 were obtained. In the non-linear calculations two different alternatives for the steel - concrete interface were studied. In the first one slip in the interface between steel and concrete was ignored (rigid link), in the second one the flexibility of the shear studs (based on results by Lebet in Kürschner *et al.* (2005), similar results as in Ollgaard, *et al.* (1971)) was taken into account by using nonlinear springs. In the first step the nonlinear calculation was limited to the most unfavourable traffic load case for the section m at midspan (Fig. 7), because the utilisation of the plastic moment capacity was primarily focused on that section.

It is worth mentioning how the determination of the bending stiffness in the side spans was carried out. The contribution of the concrete slab in the side spans was taken into account, in contrast to Ducret and Lebet (2001). The reason for this on the one hand was to eliminate an underestimation of the moment redistribution. On the other hand the actual values of the tension stresses in the concrete slab - nearly over the whole length - turned out to be smaller than the mean value of the tensile strength ($f_{ctm} = 2,9 \text{ N/mm}^2$) so that full cracking is not to be expected. This is shown in Fig. 8 for the concrete stresses in the centre line of the slab for different levels of the traffic load. In addition, the fractile values of the concrete tensile strength are illustrated in the diagram ($f_{ct0,95} = 3,77$ and $f_{ct0,05} = 2,03 \text{ N/mm}^2$). Even if additional effects are taken into account, such as creep and shrinkage, stages and sequence of

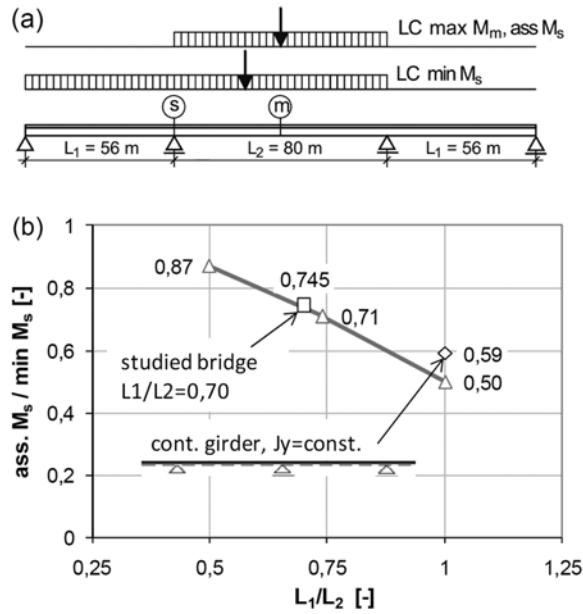


Fig. 7 (a) Relevant traffic load cases for the studied cross sections m and s . (b) Ratio between associated and minimum moment at internal support (s).

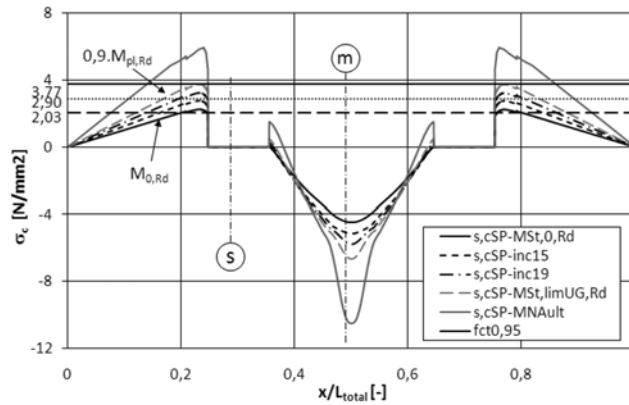


Fig. 8 Nonlinear global analysis for the most unfavourable load case at midspan m ; Tension stresses in the concrete slab at the centre line of the concrete slab

construction, the above assumption seems more likely than a bending stiffness based on a fully cracked slab.

3.2 Results of the nonlinear calculation

Before the results of the nonlinear calculations are shown, some remarks on the assumed loading with regard to a fully consistent representation. The dead loads, acting on the structural steel section only,

were increased to reach a high utilisation for the top flange, but - also for the governing traffic loads of the Eurocode - elastic behaviour throughout the bridge length should be obtained. This assumption leads to a preload level of $g_d = 150 \text{ kN/m}$, which is about 10% less than for the studies of the plastic section capacity in chapter 2. Afterwards the level of the relevant traffic load case (Fig. 7) was increased in the nonlinear analysis. The effects of the dead load, acting on the composite section (e.g., asphalt surface), is indirectly considered in the increased preload. For the main results of this study these simplifications are not relevant.

In Fig. 9 the development of the bending moments at midspan (section m) and at the internal support (section s) are illustrated, when the most unfavourable traffic load case for section m (Fig. 7(a)) is raised. The moments are plotted on the vertical axis against the vertical deflection at midspan on the horizontal axis (traffic load model ÖNORM (1970) and RVS (1999) with heavy duty vehicle of 150 tons). In addition, the bending capacities of the composite section (elastic: $M_{e,Rd}$, plastic: $M_{pl,Rd}$) and the value $M_{0,Rd}$ based on the elastic approach in Fig. 1 are plotted. The moment capacity $M^*_{S,pl,Rd}$ of the internal support is an upper limit for a slender stiffened section, when yielding is reached on the bottom

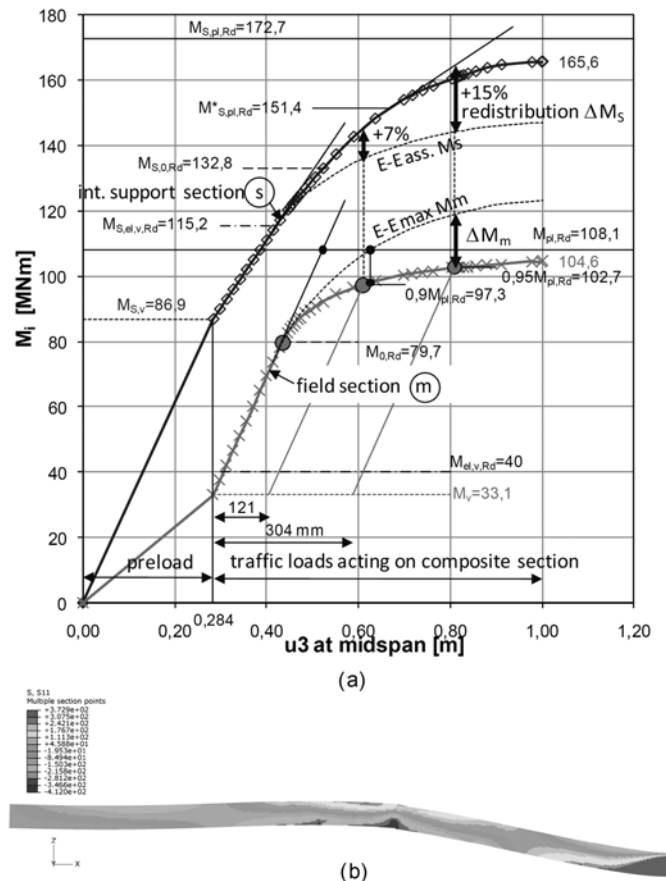


Fig. 9 Nonlinear global analysis for the most unfavourable traffic load case at midspan. (a) Development of the bending moments at midspan (m) and at the internal support (s) related to the vertical deflection at midspan, (b) Deformations and normal stresses at ultimate load.

flange, after minor plastic stress redistribution in the upper tension zone occurs.

One important result of Fig. 9 is that increased bending moments close to the plastic section capacity $M_{pl,Rd}$ lead to very high vertical deformations. These would also remain, to a large extent, if traffic loads are removed (unloading is nearly elastic) and thus would change the gradient of the bridge deck significantly. For example, if the bending moment reaches 90% of $M_{pl,Rd}$ a vertical deformation of 61 cm would occur and after removal of the traffic loads 12 cm would remain. For a bending moment of 95% $M_{pl,Rd}$ the vertical deformation is 81 cm, so that about 30 cm would remain after the traffic load is removed (this means a ratio of $L / 270$).

The high vertical deformations also lead to high horizontal movements at the bearings in longitudinal direction. Based on the assumption of a fixed bearing at one abutment, the load increase to a bending moment of 90 / 95% $M_{pl,Rd}$ leads to horizontal movements of about 35 / 47 mm, which would usually exceed the design values.

Another important aspect is the moment redistribution due to utilisation of plastic effects at midspan. In Fig. 9 also the associate moment at the internal support is plotted above the moment at midspan, assuming elastic behaviour there. In comparison with the correct moment at the internal support the moment redistribution ΔM_s from the midspan to the internal support is visible. Expectedly, this redistribution starts when the yield limit at the midspan section ($M_{0,Rd}$) is exceeded, and the increase is very disproportionate if the bending moment at midspan approaches the plastic capacity. For example, if the bending moment at midspan reaches 90% of $M_{pl,Rd}$ the increase of the moment at the internal support is about $\Delta M_s = +7\%$, but reaching 95% of $M_{pl,Rd}$ leads to $\Delta M_s = +15\%$. The latter increase cannot be seen directly in Fig. 9, because at that high traffic load level the calculation would indicate yielding also in the section at the internal support, resulting in smaller moments. Therefore, a simplified linear extrapolation, starting with $M_{S,pl,Rd}^*$, was made in Fig. 9.

Based on these results now the question arises, to which extent the section at the internal support can take over this moment increase ΔM_s , if the section capacity there is elastic.

3.2.1 Checking of the section at the internal support

For evaluation of this question, it must be checked at the internal support whether the difference between minimum bending moment (Fig. 7) and associate bending moment (for most unfavourable traffic load case at midspan) - both based on an elastic global analysis - is higher than the moment redistribution ΔM_s due to plastification at midspan.

In Fig. 10 all the relevant aspects are summed up for the studied bridge structure (based on the national traffic load model ÖNORM (1970) and RVS (1999), with the heavy duty truck of 150 tons). Both the linear elastic and the nonlinear calculations for the most unfavourable traffic load case at midspan and that at the internal support are given. The development of the bending moments is plotted on the vertical axis against the level of the traffic loads (load amplification factor LAF). On the one hand the maximum moment at midspan and the associate moment at the internal support are presented (load case max M_m / ass M_s) and on the other hand the minimum moment at the internal support and the associate moment at midspan (load case min M_s / ass M_m). A comparison of the bending moments between the two sections is possible along vertical lines, because of identical load levels. As long as the maximum moment at midspan max M_m is lower than the elastic capacity of the composite section $M_{0,Rd}$, the associate moment at the internal support ass M_s is significantly smaller than the relevant moment for design min M_s . Increasing the utilisation of the plastic section capacity at midspan leads to a convergence of ass M_s and min M_s . At an utilisation level of 94% of $M_{pl,Rd}$ at midspan the associate moment ass M_s is significant for design (ass $M_s = \min M_s$). Looking at the curve for min M_s in that

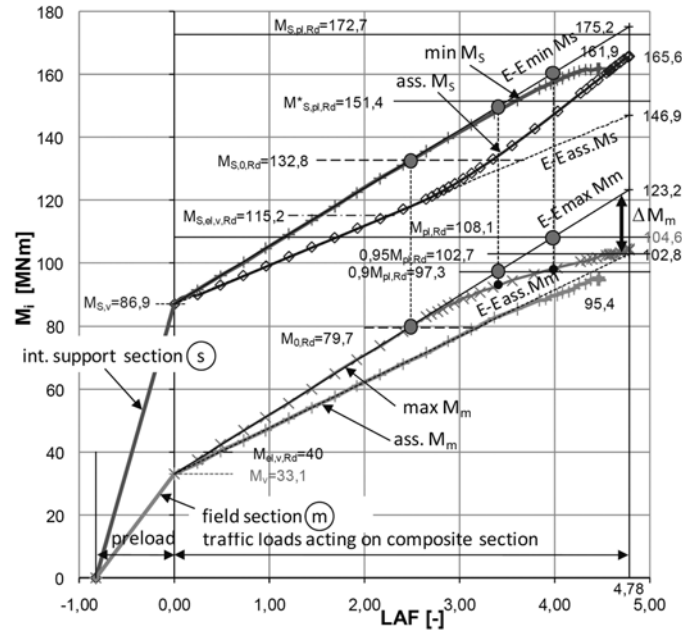


Fig. 10 Nonlinear global analysis for cross section m and s . Development of the bending moments, depending on the traffic load amplification factor LAF.

region shows that the plastic section capacity at the internal support is also utilised. Since this is not tolerable for a slender section strengthening of this section would be necessary in practice. This would then lead to the plotted curve extrapolation in Fig. 10 (E-E min M_s).

Summarising this example, the full plastic moment at midspan can be reached, without exceeding the elastic moment min M_s at the internal support, based on a common elastic global analysis. In view of refurbishment of old bridges with increased (traffic-) loads, therefore, only the region around the internal supports would have to be strengthened, whereas in the span the utilisation of the plastic bending resistance is possible.

Finally another question arises: i.e., whether these results can be generalised for other span ratios L_1 / L_2 . With regard to this question Fig. 7(b) is helpful, since it shows the moment ratio $\text{ass } M_s / \text{min } M_s$ at the internal support against the span ratio. It is simplified for constant bending stiffness over the bridge length and for bridges with three spans overall. In addition, the studied example is plotted as well as a continuous girder with many spans. The consistency of all results allows the conclusion to a more general behaviour, including more than three spans and varying bending stiffness. It can be seen that the approach to equal adjacent spans is connected with a significantly higher moment redistribution for the section at midspan. In contrary, approaching span ratios smaller than 0,6 would limit the redistribution to just about 20%.

3.2.2 Other vulnerable sections

Up to this point the focus regarding overstraining when utilising the plastic moment at midspan was limited to the internal support. Now, all the other sections are checked and the relevant positions in longitudinal direction are given for critical sections. With regard to this, the envelope curves of the extreme bending moments due to traffic loads in every section are needed. For the traffic load model of

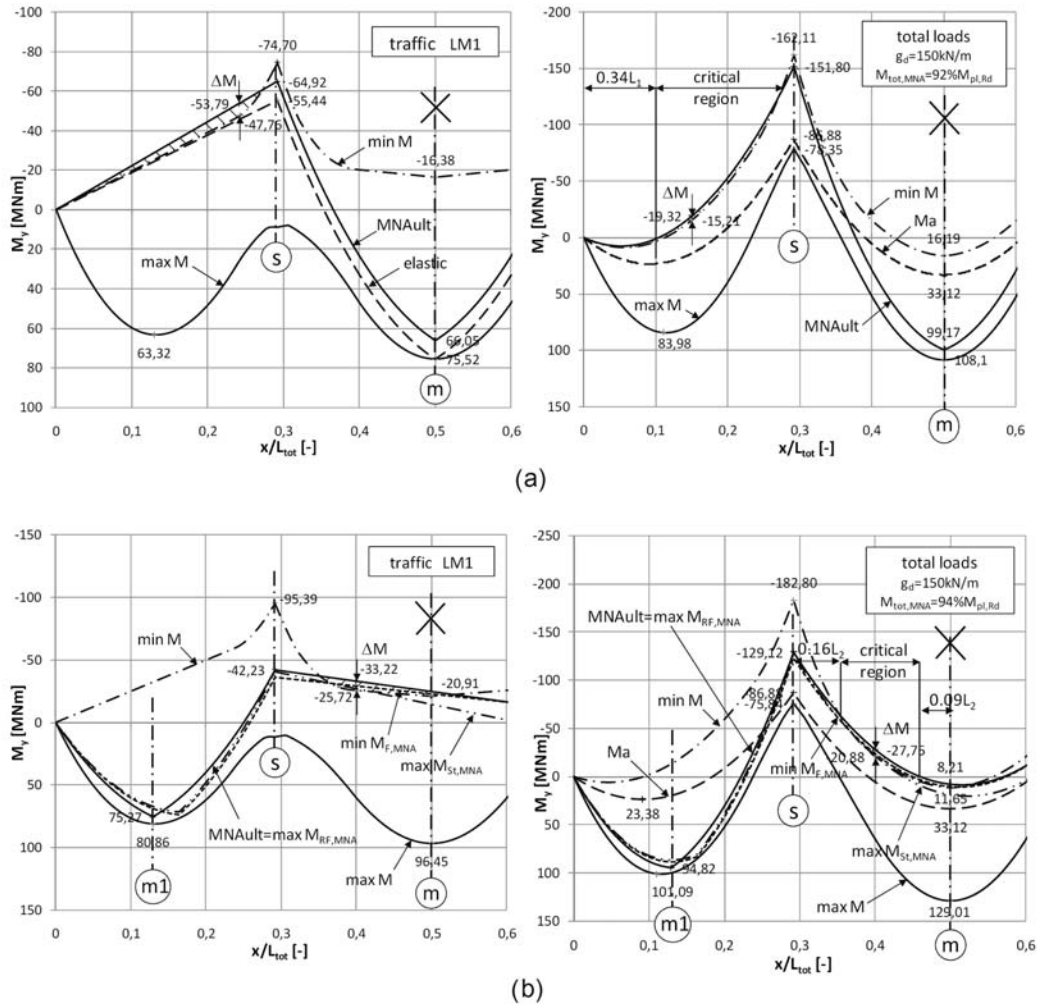


Fig. 11 Critical cross sections due to redistribution of bending moments, if plastic utilisation in span is based on elastic moments; (a) plastic behaviour at midspan - section m , (b) plastic behaviour at section $m1$.

the Eurocode these curves (min M , max M) are plotted in Fig. 11 (diagrams on the left hand side). Utilisation of the plastic capacity in span yields to significant effects in the sections of the adjacent spans, when being without traffic loads. There the moment redistribution increases the minimum moments. Critical sections can be found if the moment diagram for the nonlinear global analysis MNA_{ult} lies above the envelope curve min M based on an elastic global analysis.

When looking at the envelope curve min M in Fig. 11, at first the midspan seems critical if utilisation of the plastic bending capacity in the side spans is considered. Therefore, an additional nonlinear calculation was made for sections $m1$ in the side span. The position of section $m1$ was varied, to maximise the moment redistribution to the main span. In total three sections were considered. For these nonlinear calculations the region near the internal support had to be strengthened to get elastic behaviour there, because the utilisation of the sections in the side span was significantly lower than in midspan.

To show the vulnerable sections beside the two elastic envelope curves (min M , max M) also the

moment diagrams for the nonlinear global analysis of the studied sections in span, based on their most unfavourable traffic load case, are plotted in Fig. 11. These curves are denoted by MNA_{ult} , for material nonlinear analysis near the ultimate load. Fig. 11(a) shows the results for section m in the main span and Fig. 11(b) shows the results for the sections mI in the side span. The diagrams on the right hand side show the total moments, whereas the diagrams on the left hand side show the moments due to traffic load only (moments due to preload are subtracted). For an objective comparison it is important that the moment envelope curve and the moment diagram imply the same traffic load level. Because the studied sections in span (m , mI) give different utilisation factors for the identical traffic load level, two individual plots are necessary, leading to different traffic load levels in Fig. 11(a) and 11(b).

In a first step a design method - as provided in Eurocode 4 (2007) - is discussed, where linear elastic bending moments are used and the plastic moment capacity is utilised in midspan. At first view it seems correct to consider the load level where the plastic moment capacity $M_{pl,Rd}$ of the sections in span (m , mI) is reached and then to use the associate envelope curve $\min M$ and curve MNA_{ult} for comparison. This approach would neglect the favourable effect of the moment redistribution of the sections in span, because the non-linear behaviour reduces the elastic moments in span ($MNA_{ult} < \max M$). This means that in design with the maximum elastic moment M_m and utilisation of the full plastic moment capacity $M_{m,elastic} = M_{pl,Rd}$ the actual utilisation factor is smaller than one (e.g., $M_{pl,Rd} = 108,1$ and $MNA_{ult} = 99,2$ kNm in Fig. 11(a)). The real moment based on the nonlinear global analysis reaches 92% (in m) and 94% (in mI) respectively.

The incomplete utilisation of $M_{pl,Rd}$ of the section in midspan is also beneficial for the section at the internal support. Therefore, the ratio of the adjacent spans L_1 / L_2 , describing the limit of possible redistribution from midspan to internal support, should be reducible to $L_1 / L_2 = 0,6$ without exceeding the minimum elastic moment there.

Regarding the vulnerable sections, if the plastic bending capacity in the spans is used, the main aspects as shown in Fig. 11 are:

On the right hand side the critical region is marked, where sections due to the moment redistribution get increased moments compared to the minimum moments based on an elastic global analysis. At first view the moment increment ΔM seems small. The percental increase is highest near the zero-point for the envelope curve $\min M$, here at a distance of $0.35 \cdot L_1$ from the abutment in the side span and at a distance of $0.4 \cdot L_2$ from the internal support in the main span. For the marked sections the percental increases are: +27% (19,3 instead of 15,2 MNm) for the section in the middle of the sidespan and +33% (27,8 instead of 20,9 MNm) in the centre of the critical region of the main span. However, the numerically significant increases should not be relevant for the design conditions in practice.

Obviously higher moment increments ΔM are obtained if the full plastic moment capacity $M_{pl,Rd}$ is utilised in midspan. This means that there the moments of the nonlinear global analysis are the bases for design. The results are shown in Fig. 12. For the same selected sections as in Fig. 11 we obtain: +53% for the section in the middle of the side span and +84% in the midspan section. Now also in the centre of the midspan we get negative (hogging) moments.

Generalising these results for bridges with a larger number of spans means that the results for the midspan are relevant for all inner spans.

In summary, it has been found that sections near the zero-point of the moment envelope - curve $\min M$ get additional hogging moment increments ΔM , even if the plastic moment capacity is not fully utilised.

3.2.3 Effects on the forces in the shear studs

The increase of the forces in the shear studs, compared to the practical elastic approach, is also worth

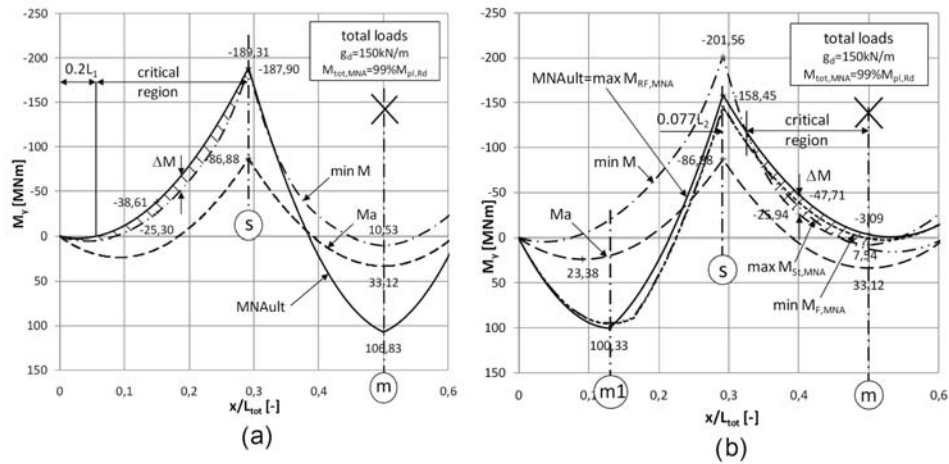


Fig. 12 Critical cross sections due to redistribution of bending moments if full plastic capacity is utilised in span; (a) plastic behaviour at midspan - section m , (b) plastic behaviour at section $m1$.

mentioning. The following results are based on a calculation with the European traffic load model (Eurocode 1 (2003)) for the midspan section m , if the full plastic moment $M_{pl, Rd}$ is reached. The slip in the interface between concrete and structural steel is considered by using nonlinear springs for the stiffness of the shear studs. In Fig. 13 the forces in the shear studs near the studied section m are plotted for different load levels in order to study the different shear force distributions. The shear - force distribution based on linear behaviour is compared with the fully plastic case (MNA_{ult}). The increase of shear forces due to the utilisation of the plastic moment capacity is shaded. Their maximum ΔP occurs at a distance of about one girder depth h_{HT} beside midspan section m . For a simplified approach an effective length of about $L_{eff} = 3,0 h_{HT}$ may be considered. Similar behaviour may be expected if other sections in span are designed for plastic behaviour.

As a consequence for design practice, if the plastic moment capacity is utilised, the increase of shear force may be accounted for by adding the compressive force ΔN_c of the concrete slab, acting on the

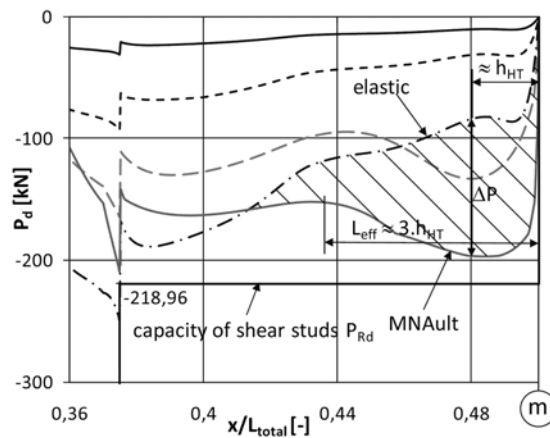


Fig. 13 Shear forces in headed stud connectors near the section m with ultimate plastic moment

length L_{eff} , to the elastic shear forces in the shear studs. ΔN_c is based on the integrated normal stresses in the slab, arising from the portion of the actual moments higher than the elastic resistance $M_{0,Rd}$.

4. Summary and recommendations for design practice

The focus of this paper is to show the potential and the consequences of making use of the plastic (sagging) moment capacity for sections in midspan of slender girders, which are composed of thin webs with longitudinal stiffeners making them susceptible to local buckling due to non-composite, locked-in compression stresses. The most important findings are:

- In the opinion of practitioners, also slender composite girders in sagging bending with high preloads can be classified as compact sections based on the plastic stress distribution of the composite section (Fig. 1). This could be confirmed in this study.

- Utilisation of nearly the full plastic moment capacity in the field section leads to disproportionately high vertical deformations and movements at the bearings, which would not fully bounce back after traffic unloading. For bridge decks in form of grids with more than two main girders high additional stresses and strains would arise in the diaphragms, if the traffic loads primarily act on one main girder (This effect has not been studied in this paper).

- The moment redistribution due to the utilisation of the plastic moment capacity in span also leads to additional hogging moments for sections near the zero - point of the moment envelope curve $\min M$ of the adjacent span. For sections near the internal support these effects are covered by the moment difference $\Delta M = \min M_s - \text{ass} M_s$ as long as the ratio of the adjacent spans $L_1 / L_2 > 0,6$, as stated in Ducret and Lebet (2001).

- If the design of the sections is based on an elastic global analysis and utilises the full plastic moment capacity in the span, the real utilisation is smaller due to the favourable moment redistribution (about 92-95% for the studied sections m and mI).

Based on these results, it is not recommended that the the full plastic moment capacity $M_{pl,Rd}$ in span is utilised for long - spanned continuous girder bridges. For design based on linear elastic bending moments utilisation of the plastic moment capacity in span can be recommended for a reduced level of about 90-95% of $M_{pl,Rd}$.

Even if the utilisation is restricted to the above limits the following aspects - at least in a simplified way - should be checked in addition to the elastic global analysis:

- additional hogging moments in the vulnerable sections near the zero - point of the moment envelope curve $\min M$

- additional horizontal deformations at the moveable bearings
- additional shear forces in the shear studs near the midspan section
- possible strains at diaphragms for bridge decks with more than two main girders

Based on these results, additional comprehensive studies for similar bridges should be made to find out simple rules for the effects of the moment redistribution, in such a way that an elastic global analysis is sufficient for the design process. Thereby it should be verified if an utilisation of the plastic sagging moment capacity is also possible for sections near the internal supports.

References

- ABAQUS (2007), Software package, Version 6.7.
- Chen S. and Jia Y. (2008), "Required and available moment redistribution of continuous steel-concrete composite beams", *J. Constr. Steel. Res.*, **64**(2), 167-175.
- Couchman G. and Lebet J.P. (1996), "A new design method for continuous composite beams", *Struct. Eng. Inter.*, **6**(2), 96-101.
- Ducret J.M. and Lebet J.P. (2001), "Plastic design of composite bridges", *Stahlbau*, **70**(1), 26-37
- EBPlate (2006), Software package, www.cticm.com, CTICM.
- Eurocode 1, European Standard (2003), *Actions on structures, Part 2: Traffic loads on bridges*, EN 1991 - 2.
- Eurocode 3, European Standard (2007), *Design of steel structures, Part 1-5: Plated structural elements*, EN 1993 - 1 - 5.
- Eurocode 4, European Standard (2007), *Design of composite steel and concrete structures, Part 2: General rules and rules for bridges*, EN 1994 - 2.
- Fournier A., Picard A. and Massicotte B.(1994), "Ultimate strength of slender composite steel plate girder", *Developments in short and medium span bridge engineering, Halifax*.
- Johansson B., Maquoi R and Sedlacek G.(2001), "New design rules for plated structures in Eurocode 3", *J. Constr. Steel. Res.*, **57**(3), 279-311.
- Johnson R.P. and Chen S. (1991), "Local buckling and moment redistribution in class 2 composite beams", *Struct. Eng. Inter.*, **1**(4), 27-34.
- Johnson R.P. and Huang D. (1995), "Composite bridge beams with mixed – class cross sections", *Struct. Eng. Inter.*, **5**(2), 96-101.
- Kürschner K. and Kuhlmann U.(2005), "Mechanical shear connections for composite steel and concrete girders", *Stahlbau Kalender*, **7**, Ernst & Sohn, (in German).
- Lääne A. and Lebet J.P. (2005a), "Design of slender composite bridges considering available support region rotation capacity", *Struct. Eng. Inter.*, **15**(2), 105-112.
- Lääne A. and Lebet J.P. (2005b), "Available rotation capacity of composite bridge plate girders under negative moment and shear", *J. Constr. Steel. Res.*, **61**(3), 305-327.
- Maquoi R. and Skaloud M. (2000), "Stability of plates and plated structures: General report", *J. Const. Steel. Res.*, **55**(1-3), 45-68.
- ÖNORM B 4002 (1970), Austrian national standard, *Highway bridges, General rules for Construction*.
- Ollgaard J.G., Slutter R.G. and Fisher J.W. (1971), "Shear strength of stud connectors in lightweight and normalweight concrete", *AISC Eng. J.*, April, **8**(2), 55-64.
- RVS 15.114 (1999), Austrian guideline for traffic loads due to heavy duty vehicles, *Österreichische Forschungsgemeinschaft für Straße und Verkehr*.
- Utenthaler G (2008), "Plastic moment capacity of composite highway bridges", diploma thesis at TU Graz.